PHYSICAL REVIEW B VOLUME 50, NUMBER 4 15 JULY 1994-II

Phonon-assisted Γ-X transition rates in type-II superlattices

M. U. Erdoğan, V. Sankaran, and K. W. Kim
Department of Electrical and Computer Engineering, North Carolina State University, Raleigh, North Carolina 27695-7911

M. A. Stroscio and G. J. Iafrate
U.S. Army Research Office, Research Triangle Park, North Carolina 27709-2211
(Received 7 March 1994)

The Γ-X transition rate for electrons in type-II superlattices is calculated for the case of optical-phonon emission. The tight-binding method for electronic band structure and the dielectric continuum model for phonons are used. The relative strength of scattering due to different phonon modes is examined for varying superlattice dimensions. The scattering rate is highest when the energy separation between the Γ and X levels is smallest, and decreases quickly as the separation increases. It is found that the strongest scattering rate is due to the emission of AlAs confined modes. Changing of parity with layer thickness and its effect on scattering are discussed.

I. INTRODUCTION

Recently, there has been considerable interest in hot-carrier dynamics in heterostructures. One important issue in this area has been the relaxation of photoexcited carriers from higher-energy subbands to the lower ones. This process has been studied extensively both experimentally and theoretically because of its fundamental nature as well as for possible device applications.[1-7] Most of the work up to now has been on type-I heterostructures where the band gap of one material is entirely nested within the band gap of another material. Consequently, electrons and holes are both localized in the same layer in these structures. On the other hand, in the so-called type-II superlattices, the holes are localized in one layer, whereas the lowest-energy electrons are contained in the opposite layer.[8] This is due to the staggered band alignment in these heterostructures. The well-studied $Al_xGa_{1-x}As$/GaAs superlattices can be made type-II by appropriately choosing the layer thicknesses and alloy compositions. For example, GaAs/AlAs superlattices with thick AlAs layers are known to be type-II for GaAs layer thicknesses less than or equal to 35 Å (12 monolayers).[8] Type-I to type-II transitions can also be achieved by application of external forces such as an electric field or hydrostatic pressure. In the case of type-II structures, the lowest conduction-band level is not in the GaAs but in the $Al_xGa_{1-x}As$ layer. In type-I heterostructures, electrons photoexcited from the valence band to the conduction band relax to lower-energy levels within the same layer. However, in type-II structures, the electrons excited to a direct-gap energy level (Γ) in one layer then can relax to an indirect-gap energy level (X) in the adjacent layer. This is a very interesting case because electron relaxation occurs in conjunction with real-space transfer. This process, which is normally forbidden, is now possible due to the mixing of Γ and X states by the superlattice potential and relaxation of momentum conservation due to interface disorder (lateral mixing). Several experimental results related to Γ-X transfer are available in the literature.[5-7] In spite of the spatial charge transfer, the relaxation rate can be very high. Experimental evidence has been presented that Γ-X electron transfer occurs by the emission of long-wavelength optical phonons.[7] However, a detailed theoretical analysis for the Γ-X transfer in type-II structures has not yet been given.

In this paper, we calculate the Γ-X scattering rates due to optical-phonon emission using a realistic band-structure model and show that this is an important mechanism for the Γ-X relaxation process in type-II superlattices. The paper is organized as follows. In Sec. II, we present the tight-binding model and the dielectric continuum model used in the calculation. Evaluation of matrix elements is explained. In Sec. III, we present and discuss our results of electron relaxation rates. Finally, in Sec. IV, a summary is given.

II. FORMULATION

It is well known that the electron–optical-phonon interaction in low-dimensional systems can be altered strongly due to the confinement of the carriers and the confinement of the phonons. Usually, a single-band, spherical effective-mass model is used for the description of the confined carrier states. It is commonly assumed that each of these states is derived from bulk states of a given symmetry only (e.g., Γ, X, or L), and levels derived from different bulk states do not interact with each other. In a superlattice, momentum in the growth direction is not conserved due to the discontinuities in the superlattice potential in this direction. Therefore, bulk states of the same energy but different symmetry can couple with each other. For a superlattice grown in the z direction, the sixfold degeneracy of the X valley is removed, with the formation of an X_z doublet having momentum along the growth axis, and an $X_{x,y}$ quadruplet, with momentum in the plane. The $X_{x,y}$ and L minima are not coupled to the Γ valley due to the conservation of lateral momentum. Therefore, only the Γ and X_z valleys are coupled

0163-1829/94/50(4)/2485(7)/$06.00 ©1994 The American Physical Society

through this potential. Accordingly, out of all the X states, only the X_z states are mixed with the Γ states by the perfect superlattice potential, and, herein, the X point will be used specifically to mean X_z. As a result of this coupling, the confined states are made of more than one bulk state and the electronic band structure is more complicated in type-II superlattices. Therefore, the envelope-function approximation, which works very well in many cases, is not suitable in this case. The basic assumption of the envelope function approach is that the zone center periodic parts of electronic wave functions do not differ significantly between the materials composing the heterostructure. This assumption is no longer valid in type-II superlattices since the band extrema in the different materials lie at the different points in the Brillouin zone. In type-II superlattices, a model for band structure that can handle the mixing between different valleys is needed. Several such methods have been employed in the literature.[9–14] In this study, an empirical tight-binding method with an sp^3 basis is used for describing the electronic band structure.[15,16] The mixing of the Γ and X valleys is included intrinsically in this model since the complete band structure is described in the tight-binding method. In the tight-binding method, the wave function is built up from atomiclike orbitals:

$$\psi_n(\mathbf{k},\mathbf{r})=\sum_i \sum_\alpha c_{n,i,\alpha}(\mathbf{k})\frac{1}{\sqrt{N}}\sum_a e^{i\mathbf{k}\cdot(\mathbf{R}_a+\mathbf{r}_i)} \times \xi_{i,\alpha}[\mathbf{r}-(\mathbf{R}_a+\mathbf{r}_i)] , \quad (1)$$

where n indicates the band, i indexes the ions in the unit cell, α designates the orbitals (i.e., s, p_x, p_y, and p_z for the anion and the cation), $c_{n,i,\alpha}$ are expansion coefficients, N is the number of unit cells in the crystal, a indexes the Bravais lattice sites of the crystal, $\mathbf{R}_a$ is the corresponding lattice translation, and $\mathbf{k}$ is the electron wave vector. In this equation $\mathbf{r}_i$ and $\xi_{i,\alpha}$ denote the relative position of the ith ion within the unit cell and the atomiclike orbitals centered at the ith ion, respectively. The above equation applies to both bulk materials and superlattices as long as the unit cells are chosen appropriately. In the superlattice, the unit cell should cover one period along the growth direction. For a superlattice, we refer to the expansion coefficients $c_{n,i,\alpha}(\mathbf{k})$ as the envelope functions. The atomic orbitals making up the tight-binding wave functions satisfy the orthonormality condition:

$$\int_{V_e} d\mathbf{r}\, \xi^*_{i,\alpha}[\mathbf{r}-(\mathbf{R}_a+\mathbf{r}_i)]\xi_{i',\alpha'}[\mathbf{r}-(\mathbf{R}_{a'}+\mathbf{r}_{i'})] =\delta_{\alpha,\alpha'}\delta_{i,i'}\delta_{a,a'} . \quad (2)$$

In this calculation, first and second nearest-neighbor interactions are retained. The parameters used in the tight-binding calculation are taken from Ref. 9. These parameters were optimized to reproduce the highest valence band and lowest conduction band accurately. The parameters across an interface are taken as the average of the values from the two bulk regions. The impact of not knowing the parameters across the interface exactly was minimized by using a minimum number of cross-interface parameters. The superlattice band structure is not sensitive to these parameters except for very small layer thicknesses. The spin-orbit coupling and camel-back features of the X band are neglected, since these will not affect the Γ-X mixing. The X states in the plane of the interface ($X_{x,y}$) are not coupled to the Γ states by the perfect superlattice potential. However, these X states are mixed with the Γ states by interface disorder.[13] Obviously, this effect will be more important for very short period superlattices. Interface disorder effects are not taken into account in this study.

For proper calculation of the electron–optical-phonon scattering rates, the effects of phonon confinement should also be taken into account. It is well known that the vibrational modes in low-dimensional structures are different from those in the bulk. Microscopic lattice-dynamical models have been used with great success to model these phonon modes.[17,18] However, using these models in the calculation of electron-phonon interactions requires intensive computation. Therefore, for the description of optical-phonon confinement, the dielectric continuum (slab) model employing electromagnetic boundary conditions is used in this work because of its simplicity and reasonable accuracy.[19–21] The electromagnetic boundary conditions ensure the continuity of the electrostatic potentials and are based on having continuous tangential components of the electric field as well as continuous normal components of the displacement fields across the interface. This model predicts the existence of confined longitudinal-optical (LO) phonon modes for both layers and several interface modes due to the dielectric discontinuity between the two media. There is no dispersion for confined phonon modes in this model, and the frequency of each confined mode is taken to be identical to the zone-center frequency of the bulk LO phonon. At the same time, these modes are totally confined within an individual layer, and the phonon potential of one type of layer is identically zero in the adjacent layer. Hence, phonon potentials in each well do not interact with each other, and consequently, confined phonon modes in a superlattice may be expected to be similar to those for a quantum well in this picture.

Figure 1 shows a schematic drawing of the band-edge alignment of a type-II superlattice grown in the z direction. The thickness and dielectric constant of material I (II) are denoted by d_1 (d_2) and ϵ_1 (ϵ_2), respectively. The

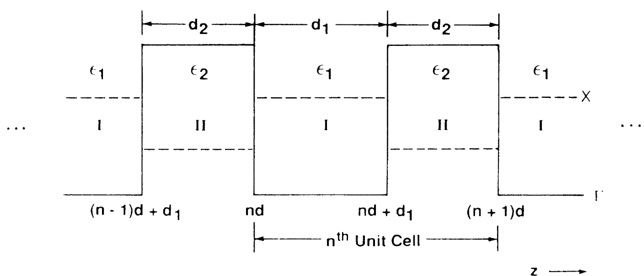

FIG. 1. Schematic drawing of the band-edge alignment of a type-II superlattice grown in the z direction.

electron–optical-phonon interaction Hamiltonian in this structure can be expressed as an expansion of the scalar potential in terms of the normal modes as follows:[21]

$$H=\sum_{\mathbf{q}_\parallel}(-e)e^{i\mathbf{q}_\parallel\cdot\boldsymbol{\rho}}\phi(\mathbf{q}_\parallel,z)(a_{\mathbf{q}_\parallel}+a^\dagger_{-\mathbf{q}_\parallel}) . \quad (3)$$

Here, $a^\dagger_{-\mathbf{q}_\parallel}(a_{\mathbf{q}_\parallel})$ is the creation (annihilation) operator, ϕ is the electrostatic potential, and $\mathbf{q}_\parallel$ and $\boldsymbol{\rho}$ are the two-dimensional phonon wave vector and position vector in the x-y plane, respectively. The electrostatic potentials for the confined modes of material I are given by[19]

$$\phi_{C_1}(\mathbf{q}_\parallel,z)=\left[\frac{e^2\hbar\omega_{L_1}}{ANd_1\epsilon_0}\right]^{1/2}\left[\frac{1}{\epsilon_1(\infty)}-\frac{1}{\epsilon_1(0)}\right]^{1/2}\times\begin{cases}\sin[m\pi(z-nd)/d_1]/[q_\parallel^2+(m\pi/d_1)^2]^{1/2}, & nd<z<nd+d_1, \quad m=1,2,3,\dots,\\ 0, & nd+d_1<z<(n+1)d,\end{cases} \quad (4)$$

where A is the cross-sectional area in the x-y plane, N denotes the total number of unit cells, and n indexes the unit cells. The confined phonon frequency ω_{L1} is taken to be identical to the bulk LO phonon frequency at the center of the zone. The Hamiltonian for the confined modes of material II is given by a similar expression. The interface phonon modes in a superlattice, on the other hand, are modified due to the periodicity of the structure and the overlapping of potentials.[19,20] In this case, the phonon potential extends over the whole superlattice. The resulting Hamiltonian due to interacting interface modes is very complex. To simplify the calculations, in this work, we derive the Hamiltonian for interface modes only for the case of $q_z=0$. The phonon-dispersion relations obtained with this condition are as follows:

$$\epsilon_1\tanh\left[\frac{1}{2}q_\parallel d_1\right]+\epsilon_2\tanh\left[\frac{1}{2}q_\parallel d_2\right]=0 , \quad (5)$$

for symmetric modes, and

$$\epsilon_1\coth\left[\frac{1}{2}q_\parallel d_1\right]+\epsilon_2\coth\left[\frac{1}{2}q_\parallel d_2\right]=0 , \quad (6)$$

for antisymmetric modes. Typical dispersion relations for symmetric and antisymmetric interface modes are shown in Fig. 2. In this figure, the interface phonon frequencies do not go to the bulk frequencies of the constituent materials as $q_\parallel$ goes to zero. For the general case of $q_z\neq0$, they do approach bulk vales at the zone center.[19] The deviation of the dispersion curve with $q_z=0$ from the dispersion curve with small but nonzero q_z is significant only when $q_\parallel$ is small. These phonon modes are not excited in the intersubband transition because the excess energy of the scattered electron permits only relatively large $q_\parallel$ phonons to be emitted in this process. Therefore, the values of the dispersion relations with $q_z=0$ and with small but nonzero q_z are very close to each other for the $q_\parallel$ range of interest here. Accordingly, the dispersion relations from the above equations are appropriate for our purposes. The electrostatic potential of the symmetric interface mode (with $q_z=0$) is given by

$$\phi_{IF}^S(\mathbf{q}_\parallel,z)=\left[\frac{\hbar e^2}{\epsilon_0 A}\right]^{1/2}\left[\frac{\partial\epsilon_1}{\partial\omega}\tanh\left[\frac{1}{2}q_\parallel d_1\right]+\frac{\partial\epsilon_2}{\partial\omega}\tanh\left[\frac{1}{2}q_\parallel d_2\right]\right]^{-1/2}\frac{1}{\sqrt{2q_\parallel}}e^{i\mathbf{q}_\parallel\cdot\boldsymbol{\rho}}(a_{\mathbf{q}_\parallel}+a^\dagger_{-\mathbf{q}_\parallel})\times\begin{cases}\cosh[q_\parallel(z-(nd+d_1/2))]/\cosh(q_\parallel d_1/2), & nd<z<nd+d_1,\\ \cosh[q_\parallel(z-(nd+d_1+d_2/2))]/\cosh(q_\parallel d_2/2), & nd+d_1<z<(n+1)d .\end{cases} \quad (7)$$

An expression analogous to Eq. (7) can be obtained easily for the antisymmetric interface modes. Figure 3 shows a typical interface phonon potential for the symmetric and antisymmetric modes.

Having obtained the appropriate electronic states and phonon modes, the electron-scattering rate due to optical-phonon emission is calculated by using Fermi's "golden rule:"

$$W_{mn}(\mathbf{k})=\frac{2\pi}{\hbar}\sum_{\mathbf{k}'}|H_{mn}(\mathbf{k},\mathbf{k}')|^2\delta(E_f-E_i+\hbar\omega) , \quad (8)$$

where $H_{mn}(\mathbf{k},\mathbf{k}')$ is the matrix element, $m\,(n)$ indicates the initial (final) subband, and $\mathbf{k}$ (E_i) and $\mathbf{k}'$ (E_f) are the initial and final wave vectors (energies), respectively. The temperature is taken to be close to 0 K and the phonon occupation number is taken to be very small. Under this condition, the matrix element, $H_{mn}(\mathbf{k},\mathbf{k}')$, is obtained as follows:

$$H_{mn}(\mathbf{k},\mathbf{k}')=\sum_{i,i'}\sum_{\alpha,\alpha'}c^*_{n,i',\alpha'}(\mathbf{k}')c_{m,i,\alpha}(\mathbf{k})\sum_{a,a'}e^{-i\mathbf{k}'\cdot(\mathbf{R}_{a'}+r_{i'})}e^{i\mathbf{k}\cdot(\mathbf{R}_a+\mathbf{r}_i)}\times\int_{V_c}d\mathbf{r}\,\phi(\mathbf{r})\xi_{i',\alpha'}[\mathbf{r}-(\mathbf{R}_{a'}+\mathbf{r}_{i'})]\xi_{i,\alpha}[\mathbf{r}-(\mathbf{R}_a+\mathbf{r}_i)] . \quad (9)$$

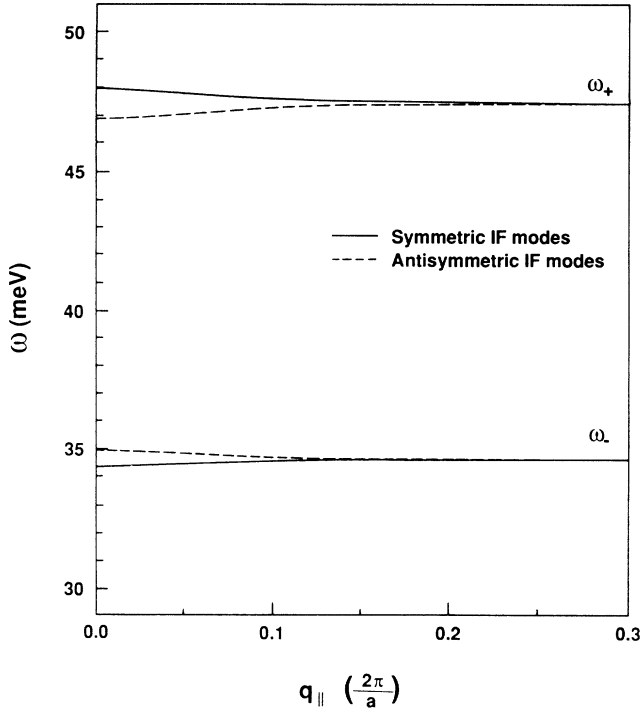

FIG. 2. Dispersion relations for the symmetric and antisymmetric interface modes for a superlattice of 8 monolayers of GaAs and 12 monolayers of AlAs with $q_z=0$.

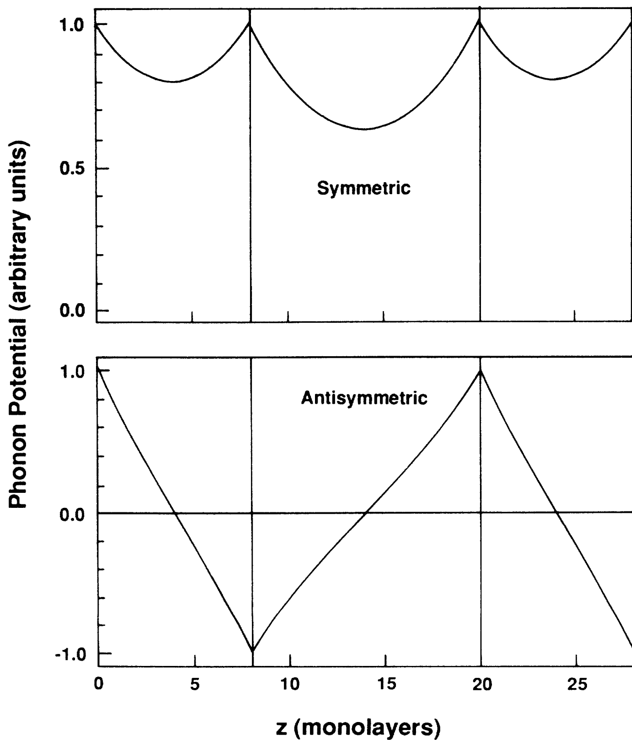

FIG. 3. Electrostatic potentials for the symmetric and antisymmetric AlAs interface modes in a superlattice of 8 monolayers of GaAs and 12 monolayers of AlAs with $q_z=0$ and $q_{\|}=0.05(2\pi/a)$, where a is the lattice constant. In this figure, the first and third regions are GaAs, the second region is AlAs. One period of the superlattice is from $z=0$–20. The potentials repeat with this periodicity throughout the superlattice.

The phonon potentials vary slowly in a unit cell compared with the atomic orbitals which are localized strongly at atomic locations. Therefore, the phonon potentials can be taken out of the summation in the above equation. Due to the orthonormality of the atomic orbitals, performing the summation in Eq. (9) reduces the matrix element to the following:

$$H_{mn}(\mathbf{k},\mathbf{k}')\approx \sum_i \sum_\alpha c^*_{n,i,\alpha}(\mathbf{k}')c_{m,i,\alpha}(\mathbf{k}) \times\phi(\mathbf{R}_a+\mathbf{r}_i)\delta(\mathbf{k}'-\mathbf{k}+\mathbf{q}_{\|}) \ . \quad (10)$$

The sum over all possible finite states within the two-dimensional Brillouin zone is evaluated numerically.[22] For simplicity, the interface phonon energy is taken as a constant in the energy-conservation equation since the dispersion is small. For the calculation of the Hamiltonian, however, phonon frequencies are taken to be those obtained from the dispersion relations given above.

III. RESULTS AND DISCUSSION

As a specific example, a superlattice with M layers of GaAs and N layers of AlAs is considered in this study. The lattice constant a is taken as 5.66 Å for both materials. Table I lists the band-edge values of GaAs and AlAs taken from Ref. 9. In this paper, we are especially interested in the energy range from the X point of AlAs (1.68 eV) to the X point of GaAs (2.1 eV). This is where the Γ and X bands mix strongly. In a superlattice, bulk states of same energy and parallel momentum, but of different wave vector in the z direction combine to make an electronic state. The energy levels at the miniband minimum obtained from the tight-binding calculations as a function of AlAs layer thickness are shown in Fig. 4. The GaAs layer was kept constant at 8 monolayers. The levels are labeled as Γ and X following the effective mass notation for convenience although each level is actually a combination of these two bulk states. Here, the superlattice states are named after the more dominant of the two bulk states forming them. In this figure, superlattice energy levels mainly derived from the same bulk states are connected with lines for easier visualization. Due to this, it may appear as if the levels cross at certain points. However, the levels actually do anticross due to the mixing effects included in this calculation. This happens when the two levels with the same parity become very close in energy. A careful examination of Fig. 4 reveals that these levels actually repel each other. As can be seen, the effect of changing the AlAs layer thickness is to make the energy difference, and accordingly, the interaction between the lowest Γ level and the X levels vary.

TABLE I. Band-edge values for the Γ and X points in GaAs and AlAs. Zero point for the energy reference is the top of the GaAs valence band.

Band edge	GaAs (eV)	AlAs (eV)
Γ	1.52	2.58
X	2.1	1.68

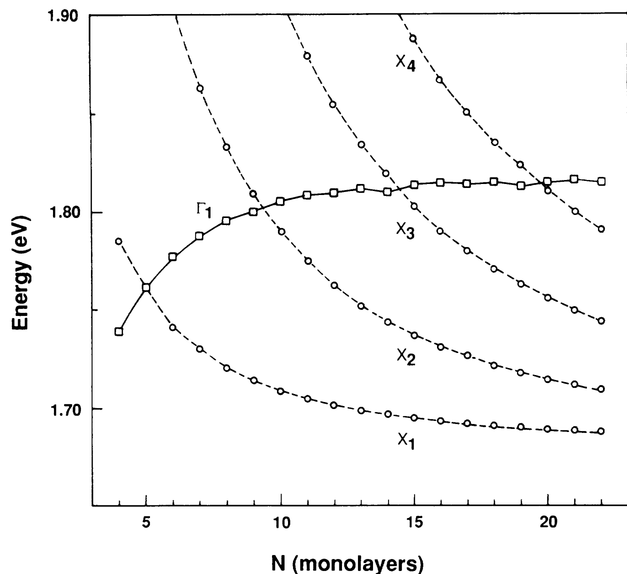

FIG. 4. Energy levels obtained from the tight-binding calculation as a function of AlAs layer thickness. The GaAs thickness is constant at 8 monolayers. The discrete energy levels are marked as Γ (squares) and X (circles) after the more dominant one of the two bulk states making up the confined state.

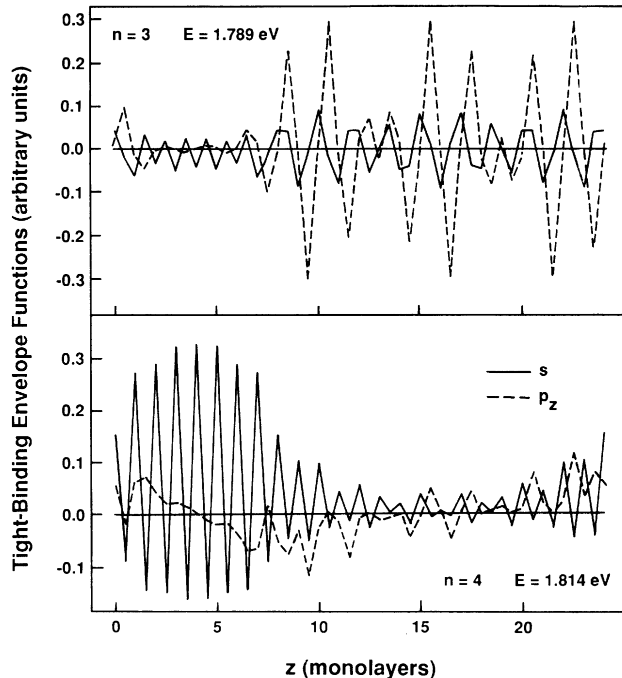

FIG. 5. Tight-binding envelope functions for a $(\mathrm{GaAs})_M/(\mathrm{AlAs})_N$ superlattice of $M=8$ and $N=16$ with $\mathbf{k}=0$. In this case, the p_x and p_y components vanish. The origin of the coordinate system ($z=0$) is located at an As plane which is followed by M monolayers of GaAs and N monolayers of AlAs.

The parity behavior of states needs to be mentioned briefly because of the effect of parity on the overlap. In a superlattice, the electronic wave functions have definite parity only when the electrons are at the miniband minimum or miniband maximum. The coefficients of the s (p_z) orbitals have the same (opposite) parity as the level itself.[9] When $k_z=0$ is assumed (i.e., at the bottom of a miniband), the parity of the superlattice wave function is the same with respect to the center of the barrier and the center of the well. In this case, the parity of the Γ_1 state is even, regardless of AlAs layer thickness. The parity of the X levels, on the other hand, depends on the number of AlAs monolayers. The X_i levels ($i=1,2,3,\ldots$) with odd (even) i have the same (opposite) parity as N. The parity behavior of states is important because the states of opposite parity do not mix for $k_z=0$. For $k_z\neq 0$, the electron states do not have well-defined parity and all states mix. This mixing, however, is much weaker than had their parities been the same.

Figure 5 shows the tight-binding envelope functions for the third and fourth energy levels for the superlattice of $M=8$ and $N=16$. (These energy levels correspond to X_3 and Γ_1 in Fig. 4, respectively.) As can be seen, the envelope functions have distinct Γ and X characters here. The envelope function of the fourth level is localized mostly in the GaAs layers and therefore it is Γ-like. The envelope function of the third level is X-like since it is strongly localized in the AlAs layers. For these superlattice dimensions, the energy difference between the Γ and X levels is large enough so that their interaction is small. Consequently, they can be identified as Γ-like and X-like. For the superlattice of $M=8$ and $N=14$ shown in Fig. 6,

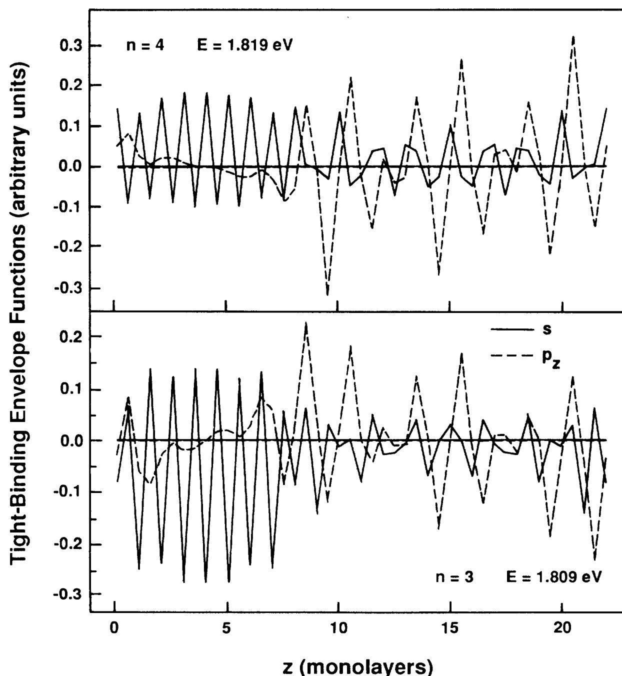

FIG. 6. Tight-binding envelope functions for a $(\mathrm{GaAs})_M/(\mathrm{AlAs})_N$ superlattice of $M=8$ and $N=14$ with $\mathbf{k}=0$. Here, p_x and p_y are zero. The coordinate system is identical to that of Fig. 5.

both the third (Γ_1) and fourth (X_3) levels have sizable Γ and X character. This is because they are very close in energy and have the same parity. The effect of parity can been seen in Fig. 7 where the envelope functions for the superlattice of $M=8$ and $N=15$ are plotted. In this case, the energy difference between the Γ and X levels is comparable with the energy difference for $N=14$. However, the parities are different. Therefore, there is no strong mixing and interaction of these states contrary to the case where $N=14$. These figures demonstrate the strong effect of changing the layer thickness on the Γ-X interaction. This strong dependence is due to the fact that thickness controls both the energy separation between Γ and X levels and the parity of X levels.

The scattering rates due to emission of different phonon modes are shown in Fig. 8. The results presented are the sum of contributions by all normal modes for a given type of phonon. In calculating the intersubband scattering rates, the electron is taken to be initially at the bottom of the lowest Γ subband (Γ_1). It then transfers to the lowest X subband (X_1) by emitting an optical phonon. As can be seen from this figure, the relaxation rates depend strongly on the AlAs layer thickness. There are two reasons for this behavior. First, the energy separation between the Γ and X levels and, hence, the Γ-X interaction, change as the thickness is varied. Second, the parities of the X levels alternate as the AlAs thickness is varied by one monolayer each time. From Figs. 4 and 8, the transition rate is strongest when the Γ and X levels are closest in energy and have the same parity. Under this condition, the levels interact very strongly with each other and the Γ level has large X character. Therefore,

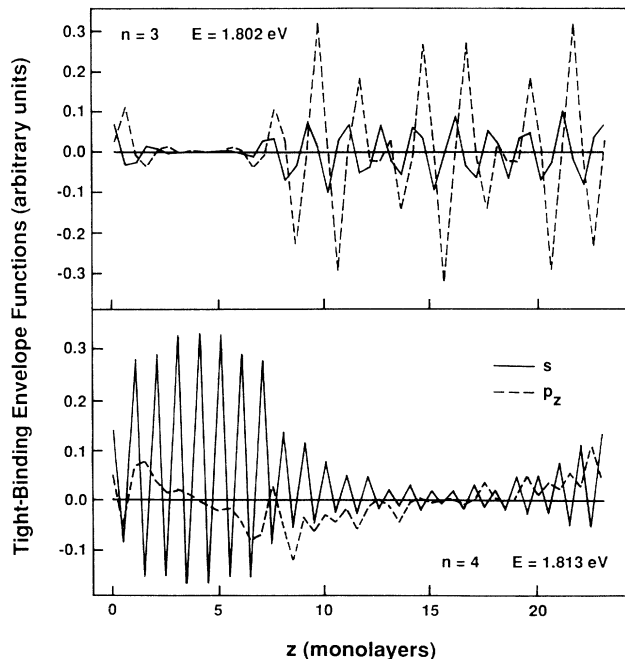

FIG. 7. Tight-binding envelope functions for a $(GaAs)_M/(AlAs)_N$ superlattice of $M=8$ and $N=15$ with $\mathbf{k}=0$. Here, p_x and p_y are zero. The coordinate system is identical to that used in Figs. 5 and 6.

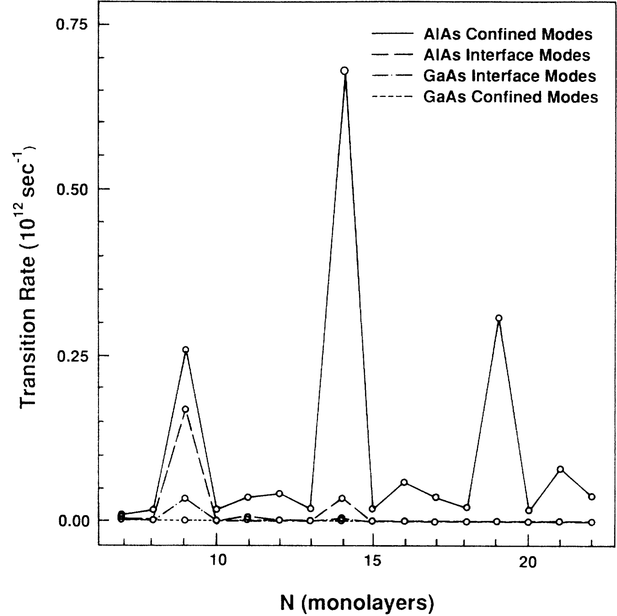

FIG. 8. Γ_1-X_1 transition rate due to optical-phonon emission as a function of AlAs layer thickness. The GaAs thickness is 8 monolayers throughout. Scattering rates due to the GaAs confined phonon modes are very small and hard to distinguish in the figure.

the overlap between the initial and final states is large. This interaction and the resulting large overlap decreases rapidly as the energy separation increases.

An interesting point to note about Fig. 8 is that the dominant phonon modes alternate between being even and odd. This is because the parity of the X level alternates each time the AlAs thickness is changed by one monolayer. For even (odd) AlAs layer thickness, parity of the lowest X level is even (odd); hence, the even (odd) phonon modes are strong. Also, the effect of parity can be observed at crossover points where the Γ and X level energies become very close. From Fig. 4, it is seen that the two levels have almost the same energy for $N=5$, but they do not mix and repel each other. This is because Γ_1 and X_1 have the opposite parity for this thickness. For other thicknesses where the two levels become close, however, they do repel each other because they have the same parity. This is the reason why the transition rate for $N=19$ is much stronger than for $N=20$. The energy separation between the Γ_1 and X_4 levels is actually smaller for $N=20$ than it is for $N=19$. However, as explained before, the parities are opposite. This results in strong (weak) mixing and transition rate for the $N=19$ ($N=20$) case. For all thicknesses considered in this paper, the AlAs confined modes are the strongest, followed by AlAs interface modes. The GaAs modes are weaker than the AlAs modes, with the GaAs confined modes being the weakest. This is due to the fact that the final state X_1 wave function is strongly confined within the AlAs layers. Consequently, the overlap involving GaAs confined modes is very small. The contributions from the interface modes become weaker as the AlAs thickness in-

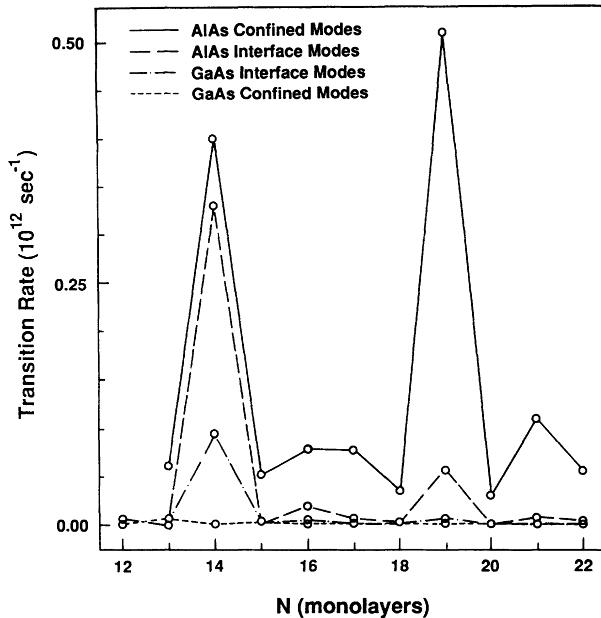

FIG. 9. Γ_1-X_2 transition rate due to optical-phonon emission as a function of AlAs layer thickness. The GaAs thickness is 8 monolayers throughout.

creases. This is similar to the case of type-I superlattices.

Depending on the layer thickness, there may be more than one X level to which the Γ electron may transfer. The relaxation rate from Γ_1 to X_2 is shown in Fig. 9. The result for Γ_1 to X_3 relaxation is similar to Figs. 8 and 9 and is not shown here. The discussion given for the Γ_1-X_1 transition applies for both these transitions as well. The results obtained here may be compared with an experiment by de Paula *et al.*,[6] where the Γ to X transition rate via phonon emission was obtained by a time-resolved anti-Stokes measurement. For the case of $M=8$ and $N=14$ (which corresponds approximately to the experimentally measured thicknesses of 23 Å and 41 Å, respectively), they found the transfer time to be around 1 ps, which is in agreement with the rate calculated in this study. However, it is very difficult to make an exact comparison due to the nature of the experiment. Another point to note is that it was not possible in their experiment to determine whether intrasubband scattering was also involved. In addition, there may be mechanisms other than optical-phonon emission for electron relaxation, e.g., carrier-carrier scattering, nonpolar optical-phonon scattering, and acoustic-phonon scattering. Besides these mechanisms, interface roughness may cause additional scattering as well.

IV. SUMMARY

The Γ-X intersubband scattering rate due to phonon emission is calculated by using the tight-binding method for electrons and the dielectric continuum model for phonons. Electron transition rates are presented as a function of AlAs layer thickness. As expected, the scattering is strongest when the levels anticross. Among the various phonon modes, the strongest are found to be the AlAs confined modes and the weakest are the GaAs confined modes. Scattering rates due to the interface modes are observed to get weaker with increasing AlAs thickness. The parity behavior of electron states and its effect on scattering are examined. The results obtained are in general agreement with the experiment.

ACKNOWLEDGMENTS

The authors would like to thank J. M. Higman for useful technical discussions. The authors are also grateful to M. Dutta for providing unpublished data on Γ-X transitions and for stimulating the initiation of the current calculations. This work was supported, in part, by the Office of Naval Research and the U. S. Army Research Office.

[1] S. M. Goodnick, J. E. Lary, and P. Lugli, Superlatt. Microstruc. **10**, 461 (1991).
[2] S. Das Sarma, V. B. Campos, M. A. Stroscio, and K. W. Kim, Semicond. Sci. Technol. **7**, B60 (1992).
[3] M. Dutta and M. A. Stroscio, J. Appl. Phys. **73**, 1693 (1993).
[4] M. C. Tatham, J. F. Ryan, and C. T. Foxon, Phys. Rev. Lett. **63**, 1637 (1989).
[5] J. Feldmann, J. Nunnenkamp. G. Peter, E. Gobel, J. Kuhl, K. Ploog, P. Dawson, and C. T. Foxon, Phys. Rev. B **42**, 5809 (1990).
[6] A. M. de Paula, A. C. Maciel, G. Weber, J. F. Ryan, P. Dawson, and C. T. Foxon, Semicond. Sci. Technol. **7**, B120 (1992).
[7] L. P. Fu, T. Schmiedel, A. Petrou, M. Dutta, P. G. Newman, and M. A. Stroscio, Phys. Rev. B **46**, 7196 (1992).
[8] For a review of work on type-II structures, see B. A. Wilson, IEEE J. Quantum Electron. **QE-24**, 1763 (1988).
[9] Y.-T. Lu and L. J. Sham, Phys. Rev. B **40**, 5567 (1989).
[10] M. A. Gell and D. C. Herbert, Phys. Rev. B **35**, 9591 (1987).
[11] D. Z.-Y. Ting and Y.-C. Chang, Phys. Rev. B **36**, 4359 (1987).
[12] T. Ando and H. Akera, Phys. Rev. B **40**, 11 619 (1989).
[13] I. Morrison, L. D. Brown, and M. Jaros, Phys. Rev. B **42**, 11 818 (1990).
[14] M. U. Erdoğan, K. W. Kim, M. A. Stroscio, and M. Dutta, J. Appl. Phys. **74**, 4777 (1992).
[15] J. C. Slater and G. F. Koster, Phys. Rev. **94**, 1498 (1954).
[16] D. N. Talwar and C. S. Ting, Phys. Rev. B **25**, 2660 (1982).
[17] H. Rücker, E. Molinari, and P. Lugli, Phys. Rev. B **45**, 6747 (1992).
[18] A. R. Bhatt, K. W. Kim, M. A. Stroscio, and J. M. Higman, Phys. Rev. B **48**, 14 671 (1993).
[19] L. Wendler and R. Haupt, Phys. Status Solidi B **143**, 487 (1987).
[20] R. Enderlein, Phys. Rev. B **43**, 14 513 (1991).
[21] N. Mori and T. Ando, Phys. Rev. B **40**, 6175 (1989).
[22] G. Gilat and L. J. Raubenheimer, Phys. Rev. **144**, 390 (1966).